Bendola Publishing
Mechanobiology Journal
Vol. 2 (2021), Article ID 246116, 15 pages
doi:10.32371/mbj/246116

Research Article

On the Role of the Reserve Zone and Mechano-Regulatory Stimuli in the Development and Maturation of the Growth Plate: Observations and Models

Masumeh Kazemi and John Williams

Biomedical Engineering Department, University of Memphis, Memphis, TN 38152, USA
Address correspondence to Masumeh Kazemi, mkzmmghd@memphis.edu

Received 29 December 2020; Revised 9 April 2021; Accepted 12 April 2021

Abstract *Background.* The subchondral epiphyseal bone plate between the epiphysis and the growth plate cartilage is formed by an unknown process. *Objective.* To examine if reserve zone chondrocytes could be involved in the development of the subchondral epiphyseal bone plate, by relating their intracellular stress-strain state to mechanobiological tissue differentiation theories. *Methods.* Multiscale elastic finite element models of the porcine proximal femoral physis at 20, 35, and 480 days after birth were created, based on histological observations. *Findings.* Simulating 15% compression of the growth plate produced intracellular maximum principal strains of 0.1–15% and compressive hydrostatic stresses of 0.15–0.4 MPa, depending on age and depth within the reserve zone. These values are within the range known to correspond with endochondral bone formation in fracture healing. Near the epiphyseal bone border the values for cellular compressive hydrostatic stress ($>$ 0.15 MPa) and maximum tensile strain (0.1%) fall in the same range as found for hypertrophic chondrocytes at the metaphyseal bone growth front. *Conclusion.* The evidence suggests that growth plate cartilage has a secondary growth front at the reserve zone-epiphysis border that contributes to forming the subchondral epiphyseal bone plate.

Keywords germinal layer; resting zone; mammillary process; elemental analysis; tissue differentiation; mechano-regulation; chondroprogenitor stem-like cells; subchondral bone; tidemark; calcified cartilage; finite element model

1. Introduction

The development and growth of much of the vertebrate skeleton, and especially the long bones, proceeds via endochondral bone formation, the process by which a cartilage precursor is gradually replaced by bone. In brief, a rudimentary cartilaginous model (anlage) of the future bone initially forms from primordial cells. The proliferating chondrocytes in the center of this anlage then differentiate and become hypertrophic after which their matrix is resorbed by invading hematopoetic and osteoblast precursor cells, forming trabecular bone and bone marrow to become the primary ossification center. This primary center expands by a complex process as the fetus grows. Somewhat later, secondary centers of ossification develop at one or both of the joint ends, which form the epiphyseal bone and articular cartilage layers. Growth cartilage gradually becomes entrapped between the expanding primary and secondary centers resulting in the formation of the epiphyseal growth plate. This layer of growth plate cartilage subsequently develops a lamellar bone plate on the epiphyseal side between the trabecular bone of the epiphysis and the growth plate reserve zone, while the metaphyseal interface continues to produce and calcify cartilage in preparation for replacement by trabecular bone. As growth continues, the shape of the epi- and meta-physeal interfaces with the growth cartilage begin to evolve three-dimensional convex or concave surfaces which in large animals become increasingly more convoluted as growth continues. These interdigitations, termed mammillary processes, have been observed at various scales, as primary, secondary and tertiary mammillary processes [1,2]. The mammillary processes provide an interlocking joint consisting of hills and valleys that continues to evolve during skeletal maturity. Such undulations also help orient the growth plate perpendicularly to directions of local principal compressive stresses to reduce tensile and shear stresses across the interfaces and provide biomechanical stability to the joint [3,4]. It is conceivable that deficiencies in the development of the subchondral bone plate and mammillary processes may result in weakening of the interface and could contribute to conditions such as slipped capital femoral epiphysis (SCFE). SCFE is characterized by a non-traumatic displacement of the femoral metaphysis with respect to the capital femoral epiphysis through failure of the physis and is believed to have a multifactorial etiology involving biomechanical, biochemical, endocrine and developmental factors [5,6,7,8,9].

Although the mechanism by which the growth plate subchondral bone plate and mammillary processes develop

is not known, it has been noted that the undulating pattern of newly formed bone on the metaphyseal side is matched by that of the epiphyseal subchondral bone (SB) plate at the growth plate reserve zone (RZ) border [3,10,11]. This suggests that modeling and remodeling of the SB plate continues throughout development as axial skeletal growth proceeds at the metaphyseal border. While little is known about the interface between the reserve zone and SB, histologically it resembles the osteochondral interface between articular cartilage and SB [12]. Articular SB has a functionally graded interlayer through which collagen fibers traverse from the deep zone of cartilage into a calcified cartilage layer [13]; the calcified cartilage consists of a series of undulating and interdigitating tidemarks that provide a mechanical interlock between the uncalcified cartilage and added layers of calcified cartilage [14,15]. Articular SB has a chemical transition zone providing a gradient in elements associated with mineralization that may help provide a buffer zone to transmit stresses across this bi-material interface. We hypothesized that a similar mechanism might exist at the osteochondral interface between the epiphyseal subchondral bone and the growth cartilage RZ.

It is known that besides biological factors the dynamic mechanical environment also provides signals to chondrocytes that are necessary for normal development and growth. The observations of Hueter and Volkmann [16, 17] that increasing and decreasing physiological levels compression across the growth plate can modulate the growth process, have led to various mechano-regulatory concepts and growth theories to explain more quantitatively how the mechanical environment may stimulate or inhibit cartilage and bone growth [16,17,18,19,20]. The effect of intermittently applied loading on tissue differentiation has been explained by a combination of two scalar components of the stress tensor, the octahedral shear (deviatoric stress) and hydrostatic stress (volumetric or dilatational stress). Hydrostatic compressive stress is believed to promote the formation of cartilage while octahedral shear stress provides a driving force for bone formation [21, 22]. Chondrocytes play a central role in the process of endochondral ossification. Their behavior is regulated by circulating hormones, local growth factors and components of the extracellular matrix. A recent multiscale model [23] has shown that the stresses and strains in chondrocytes in the proliferative and hypertrophic zones are consistent with the tissue level stresses and strains in fracture healing [22] in terms of these mechanobiology theories of bone growth. However, the role of the reserve zone (RZ) in all of this has largely been overlooked until recently. An emerging model of endochondral bone growth postulates that the RZ plays an important role in the development and growth of endochondral bones and contains a niche of skeletal stem cells. In one of the proposed schemes these RZ cells become self-renewing when stimulated by conditions in the local environment [24].

Table 1: Subject details for each age group.

Age group	Subject number	Sex	Limb	Weight (kg)
20 days old	1	Female	Right hindlimb	3.158
	2	Male	Right hindlimb	2.598
35 days old	1	Female	Right hindlimb	5.760
	2	Female	Right hindlimb	5.400
	3	Female	Left hindlimb	4.971
480 days old	1	Female	Left hindlimb	204.1

In the present study we examined the micro-structural and chemical properties across the epiphyseal bone-cartilage interface at three stages of mammillary processes development to determine if a transition zone of graded properties and a layer of mineralized cartilage with tidemarks also exists in the SB of the growth plate. We employed histology and energy dispersive x-ray spectroscopy (EDX) to analyze proximal femoral growth plate samples of domestic pigs in three age groups. EDX, a qualitative and quantitative microanalytical technique used for the identification of the elemental composition of a specimen [25,26], has been used to investigate the elemental characteristics of the different growth plate zones [27,28, 29,30], but it has not been applied to the interface at the epiphyseal-reserve zone border. We also developed a series of multiscale finite element models of growth plate cartilage to relate the mechano-regulatory concepts at the tissue and cell level in the reserve zone with the histology and EDX observations. We addressed two questions: (1) whether our histological and elemental observations at the SB interface support the hypothesis of a secondary but slower bone growth front that shapes the mammillary processes at the epiphyseal interface, and (2) whether the mechanical milieu of chondrocytes within the reserve zone is consistent with the observations of a secondary growth front in the light of prevailing quantitative mechanobiological concepts and the discovery of a niche of chondroprogenitor stem cells that can differentiate into multiple cell types including osteoblasts.

2. Materials and method

2.1. Sample preparation

Femurs were collected post-mortem from 20-, 35- and 480-day-old mixed-breed pigs (5 female and 1 male) after the completion of another study approved by the University of Memphis institutional animal care and use committee. Table 1 shows the gender and weight (kg) of the subjects in each age group. Pigs in the 20 and 480-day-old group were not subjected to any prior experimental treatment. Pigs in the 35-day-old group were used in a prior study

to examine the short-term effects of methotrexate (MTX) chemotherapy on the kidneys. MTX was injected at two time points: 14 days (4 g/kg) and 4 days (2 g/kg) before sacrifice. Although MTX chemotherapy at a high dose may cause bone growth defects in growing bones, these side effects are dosage- and duration-dependent [31,32,33,34] and we did not observe any obvious adverse effects of this treatment on the development of the growth plate in this study. All samples were sectioned along the plane bisecting the femoral neck and shaft using a low-speed bone saw (IsoMet 1000).

2.2. Histology studies

Formalin-fixed tissues were decalcified in formic acid for 7 days, embedded in paraffin, cut into 6-μm thick slices using a microtome, and stained with hematoxylin and eosin (H&E) and with Masson's Trichrome. The microstructures of the cartilage-bone interface were examined by stereo- (Olympus SZX16, Japan), bright-field- (Nikon DXM1200F, Japan), differential interference contrast (DIC) optical- (Olympus DP80, Japan) and fluorescence- microscopies. Bright-field and dark-field images were obtained at each magnification and at each image session to remove background noise by employing a macro code [35] developed for ImageJ (V1.50i, NIH) [36]. Two-dimensional cell areas near the reserve zone-epiphysis/subchondral bone (RZ-EP/SB) interface were measured using ImageJ. Higher magnification (40x) images from the interface were acquired for this purpose. We selected chondrocytes from the H&E images with stronger basophilic staining nuclei (dark purple) to compute cell areas to ensure that a major cross-sectional area of the cell was included in the histology image.

2.3. Scanning Electron microscopy and EDX

All samples were prepared following a standard protocol of tissue fixation in 2.5% glutaraldehyde in 0.1 M Na/K Tousimis-Sorensen buffer, tissue dehydration in a graded series of increasing ethanol concentrations (33, 67, 85, 95, and 100% ethanol), critical point drying, and eventually sputter-coated with a 5-nm layer of Au/Pd. Chemical and elemental studies were conducted by EDX attached to the scanning electron microscopy (SEM, NOVA NANOSEM650, Japan). Elemental line scans and map scans were obtained at a low accelerating voltage of 15 kV, a working distance of 5 mm, a low beam current of 370 pA, a spot size of 3 and an image scan size of 2048 pixels. Lower values of accelerating voltage, probe current and scan time were used to limit any further surface damage of the cartilage tissue [41]. The acquisition time was set to scan 500 points per line scan during data acquisition. Backscatter images (BE) and EDX line- and map-scans were acquired across the cartilage-bone interface to trace the major elements including Ca, P, and C and characterize spatial changes in elemental composition. At least 5 scans were collected for each age group. To remove noise and minimize spectral artifacts from line profiles and also smoothen the line profiles, a Gaussian filter was employed using a signal analyzer (MATLAB R2019a).

2.4. Statistical analyses

The widths of the elemental transition zones between age groups were analyzed using one-way ANOVA followed by post-hoc two-tailed student t-tests. Variations in the morphological parameters of chondrocytes in the RZ-EP/SB interface were evaluated using the cumulative distribution function (CDF) for each age group. The normality of cell area distributions was checked with the Shapiro-Wilk test. Due to the non-normalized distribution of the data, the nonparametric Kolmogorov-Smirnov test (KS test) was applied to compare cell areas in the RZ-EP/SB interface with those within the reserve zone within each age group. Descriptive statistics for the cell areas were calculated by log transformation to normalize the data, followed by back transformation to obtain geometric means and 95% confidence intervals. The KS test was performed with the statistical significance reported at the 95% confidence level.

2.5. Finite element analysis

To determine how mechanical stimuli regulate ossification, we modeled the growth plate during early growth as the growth plate thickness (or width) decreased from 6 mm to 1 mm between the ages of 20 to 35 days. A series of multiscale axisymmetric large deformation models were developed with ABAQUS/CAE 2019. Isotropic linearly elastic material properties were assigned to all regions of the models: epiphyseal trabecular bone (EP), calcified cartilage at the RZ border (CC), RZ, proliferative/hypertrophic zone (PZ/HZ), and calcified cartilage beyond the border of the HZ (provisional calcification, PC) and metaphysis (MP), as well as the cells and pericellular matrix (PCM) (Table 2). Each region of macroscale model (Figure 1) was meshed with four-node bilinear axisymmetric quadrilateral, hybrid, constant pressure (CAX4H) elements. We developed three microscale models (Figure 1) of cells in three different locations of the RZ to study how macroscale loads are transferred to the RZ chondrocytes and their PCM to produce cell-level mechano-regulatory signals. All cells were enveloped in a thin shell of PCM. Cell 1 represented a hypertrophic chondrocyte at 20 days in age or a large cell associated with neocartilage tissue at 35 and 480 days, located 1 mm from the RZ-EP border as observed in our histology study. Cell 2 was placed 20 μm away from Cell 1, along the axisymmetry axis, to represent the next closest chondrocyte to Cell 1. Cell 3 represented a chondrocyte located near the RZ-PZ/HZ border. Higher-order elements (CAX8H) were used to mesh the cells and

Table 2: Material properties and dimensions of the growth plate components used in the multi-scale models.

Layer	E (MPa)	Poisson's ratio	Thickness (T) in mm Radius (R) in μm
Trabecular bone at both ends of the growth cartilage	400	0.3	T6
Calcified cartilage at the RZ border	100 [37]	0.3	T0.4*
Calcified cartilage at the HZ border	50	0.3	T0.8*
RZ	0.98 [38]	0.47 [38]	T4, 3, 1, 0.5$^+$
PZ/HZ	0.49 [38]	0.47 [38]	T2, 1, 1, 0.5$^+$
Hypertrophic cell within RZ-EP border (Cell 1)/PCM	0.002 [38,23]/0.265 [39]	0.4999 [38,23]/0.45 [39]	R10*/15#
Cell within RZ (Cell 2)/PCM	0.002 [38,23]/0.265 [39]	0.4999 [38,23]/0.45 [39]	R5*/7.5#
Cell in RZ-PZ/HZ border (Cell 3)/PCM	0.002 [38,23]/0.265 [39]	0.4999 [38,23]/0.45 [39]	R5*/7.5#

*Based on the histology of a 20-day piglet femoral head. $^+$Total GP thicknesses (RZ + PZ/HZ) are 6, 4, 2, and 1 mm.
#PCM shell thickness = 0.5 × cell radius [40]. RZ = reserve zone, PZ = proliferative zone, and HZ = hypertrophic zone.

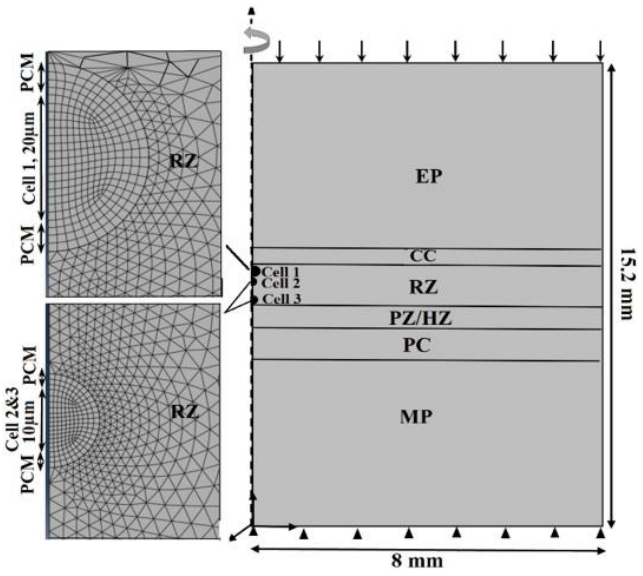

Figure 1: The idealized axisymmetric model shows tissue and cell levels for cells positioned at three locations within the RZ. The tissue was subjected to a displacement of 15% of the cartilage thickness parallel to the axis of axisymmetry. It is restrained at the bottom (in the y-direction). It includes the epiphysis (EP), subchondral bone (SB), calcified cartilage (CC), growth plate cartilage reserve zone (RZ), and proliferative/hypertrophic zone (PZ/HZ), zone of provisional calcification (PC), and metaphysis (MP). The microscale model consists of three chondrons embedded in the extracellular matrix, ECM of the RZ. All chondrons are composed of chondrocyte cells enveloped by a pericellular matrix (PCM). GP thickness = 2 mm.

PCMs, while CAX3H elements were employed for the rest of the geometry. The cylindrical growth plate model was free to expand radially while being compressed by 15% of the overall original growth plate cartilage (GP) width or thickness, along the long axis (Y) of the bone. A mesh convergence study for the microscale model was performed until further mesh refinement produced changes in the volume-average hydrostatic cell stress of 3%. An elastic model of the cartilage is relevant to fast loading conditions. Due to the assumption of a short time scale of loading, the fluid component has no time to flow through the tissue and the cartilage does not undergo stress relaxation or creep; therefore, the fluid-flow dependent behavior can be ignored. To explore the tissue and cell response with respect to mechano-regulatory concepts, the volume-averaged hydrostatic compressive stress was calculated, as described in more detail elsewhere [42,43]. Similarly, the volume-averaged octahedral shear stress and maximum principal tensile strains (logarithmic strain LE) of each cell were evaluated. The cell-averaged hydrostatic stresses and maximum principal tensile strains were used to create a quantitative tissue differentiation phase diagram similar to those proposed at the tissue macroscale level for bone fracture healing [22] and at the microscale cell level for the proliferative and hypertrophic zones of the growth plate [23].

3. Results

Evidence of the formation of the capital femoral tubercle appeared by 20 days while the secondary ossification center was still expanding toward metaphysis and before any evidence of a subchondral bone plate appeared (Figures 2(a) and 2(d)). At 20 days there were two active growth fronts producing bone on the epiphyseal and metaphyseal sides of the growth cartilage. Fifteen days later, by 35 days, the secondary ossification center had completed most if its lengthwise growth and a thin subchondral bone plate began to form on the epiphyseal side above the RZ (Figures 2(b) and 2(e)). By 35 days a prominent capital femoral tubercle had developed, which at this age may be considered a primary mammillary process (Figure 2(b)); smaller secondary mammillary processes, also began to form (arrow to the left of the tubercle). At this stage, the undulations of the epiphyseal bone—reserve zone border can be seen to closely match those of the hypertrophic zone—metaphyseal bone border. By 480 days both primary and secondary mammillary processes (black arrow and arrowhead in Figure 2(c)) had developed even further and the metaphyseal and epiphyseal

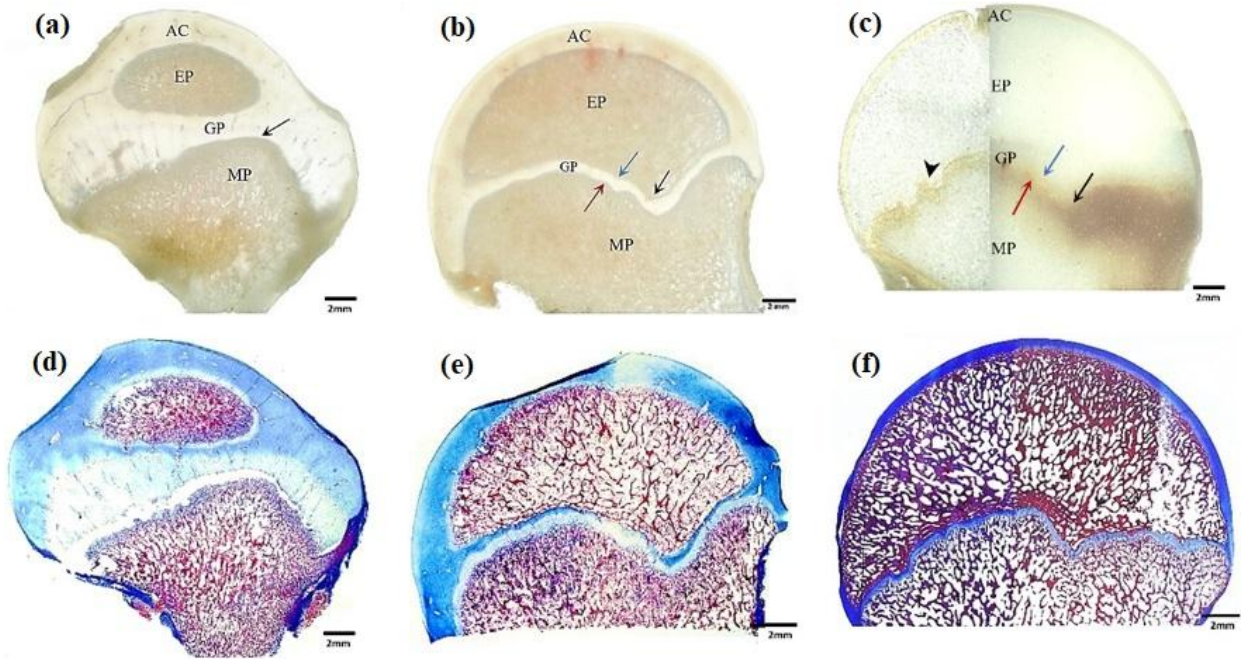

Figure 2: (a), (b), and (c) are stereo-microscopy images of a pig femoral head for three different age groups, unstained sections, which show the development of mammillary processes with age. (a), (b), and (c) are thin sections of the middle of the femoral head (cut along a plane in which the caput-collum-diaphysis angle is measured) for a 20-, 35- and 480-day-old pig, respectively. The different contrast between right and left sides of (c) is due to varying slice thicknesses. (d), (e), and (f) are sections stained with Masson's Trichrome adjacent to those of (a), (b), and (c), respectively. AC = Articular cartilage, GP = Growth Plate cartilage, EP = Epiphysis, MP = Metaphysis. Black arrows indicate the undulation of the tubercle in the femoral head; red arrows denote the metaphyseal mammillary process and blue arrows point to the epiphyseal mammillary process. Arrowhead marks secondary mammillary processes. The scale bar is 2 mm.

undulations continued to be matched, maintaining a nearly uniform thickness of the growth plate cartilage (Figure 2(f)).

3.1. Histology of the RZ-EP/SB interface

At 20 days, hypertrophic cells could be seen within the border of the RZ, belonging to the secondary center of ossification and performing similar functions to the hypertrophic cells at the metaphyseal side of the growth plate cartilage, producing calcified cartilage scaffolding to be converted later into primary spongiosa. At 20 days the growth fronts at both epi- (Figure 3(a)) and metaphyseal (Figures 3(b) and 3(c)) borders of the cartilage contained hypertrophic chondrocytes, but they were fewer in number at the epiphyseal border and lacked any evidence of a columnar zone as seen at the metaphyseal border (Figures 3(a), 3(d), and 3(g)). By 35 days, a plate-like structure of condensed bone appeared between the RZ and the epiphyseal trabecular bone (Figures 3(b), 3(e), and 3(h)). At the RZ-SB interface, clusters of cells varying in size and associated with neocartilage along the developing subchondral bone plate, accumulated near the bone marrow and tidemark (Figures 3(h) and 3(i)). Eventually, by 480 days, a thick plate of subchondral bone had developed, the tidemark had advanced and clusters of cells associated with neocartilage increased in size and number, mostly near the bone marrow becoming entrapped between multiple tidemarks (Figures 3(c), 3(f), and 3(i)). DIC microscopy afforded a clear indication of the tissue structural texture throughout cartilage-bone interface and sharply delineated the advancing tidemarks (Figure 4). The tidemark became sharper/darker and developed a more irregular wave-shape line. The higher intensity region of tidemark is more visible in oldest age group (Figures 4(b) and 4(c)).

To further document the existence of cells that appeared at locations of neocartilage within the RZ-SB interface, we looked for evidence of these in the proximal tibial growth plate of a yearling bovine calf, following the same tissue preparation protocol [12]. The EDX and histology (Figure 5) results of the bovine samples were consistent with those of the porcine growth plate. The line profile of the bovine transition zone between RZ and SB extended over 20–50 μm. The H&E stained tissue also revealed multiple tidemarks and many neocartilage nodules with closely packed cells between the epiphyseal bone marrow and growth plate reserve zone (Figures 5(a) and 5(b)). Fluorescence microscopy of H&E-stained sections showed

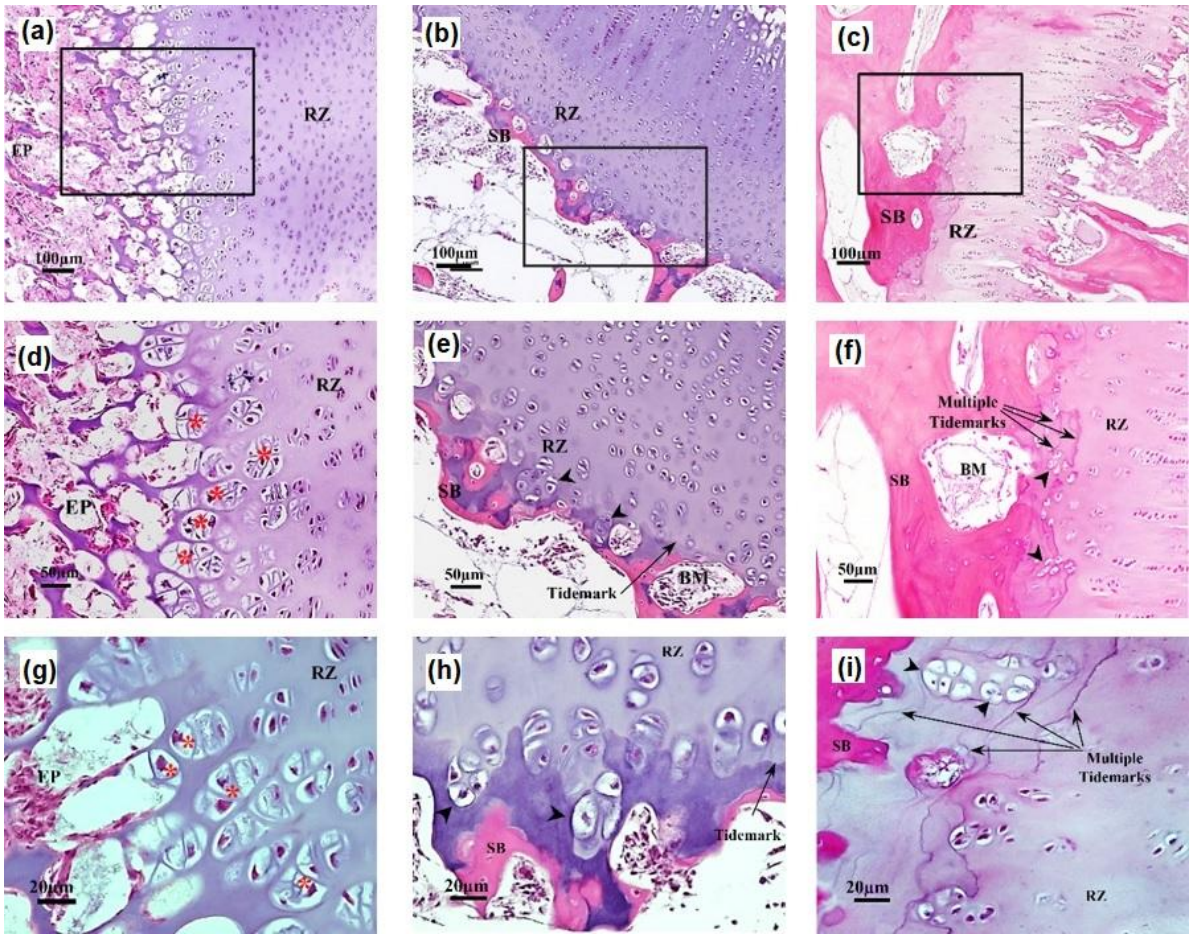

Figure 3: Histology images of reserve zone-epiphysis/subchondral bone (RZ-EP/SB) interface, stained with H&E, for the femoral head of (a) 20-, (b) 35-, and (c) 480-days-old pig. (d), (e), and (f) are magnified images of black rectangular in (a), (b), and (c), respectively. (g), (h), and (i) indicate cell features in RZ-EP/SB interface for 20-, 35-, and 480-days old pig. Red asterisks denote hypertrophic cells and black arrowheads point to cells associated with neocartilage. EP = epiphyseal bone, RZ = reserve zone, SB = subchondral bone, BM = bone marrow.

Table 3: The results of cell area measurement (geometric mean (95% CI)) for three age groups using ImageJ.

Age group	Cell area (μm^2)	
	Hypertrophic cell/cell near neocartilage in RZ-EP/SB interface	RZ cell close to RZ-EP/SB interface
20 days old	173.2 (92.3, 324.4), $n = 42$	37.13 (73.55, 18.54), $n = 49$
35 days old	93.53 (159.015, 54.54), $n = 54$	39.55 (62.11, 25.02), $n = 54$
480 days old	66.92 (106.96, 40.85), $n = 78$	29.10 (49, 15.99), $n = 80$

light regions indicative of bone tissue in the SB (Figure 5(c)) and evidence of tidemark regions corresponding to the eosinophilic tissues seen in Figure 5(b).

The RZ-EP/SB interface appeared to contain cells of various sizes, some larger than cells within the RZ proper (Table 3). By 20 days, the hypertrophic cell areas in the RZ-EP interface were about four times larger than those of reserve zone chondrocytes. For two other age groups, in which subchondral bone was present, the cell areas of cells around neocartilage nodules were double those of the RZ chondrocytes. The distribution of cell areas within the RZ-EP/SB interface followed the same pattern for all age groups (Figure 6). However, statistical analysis (KS test) indicated a significant difference for all age groups between the two groups of larger cells; one group being the hypertrophic cells at 20 days and cells associated with neocartilage at 35 and 480 days, found within the interface; and the other group consisting of the chondrocytes within the RZ proper.

3.2. Scanning Electron microscopy and EDX

Using Energy dispersive x-ray spectroscopy (EDX), we traced the distributions of some essential elements, over the areas of cartilage and bone, as well as the interfacial

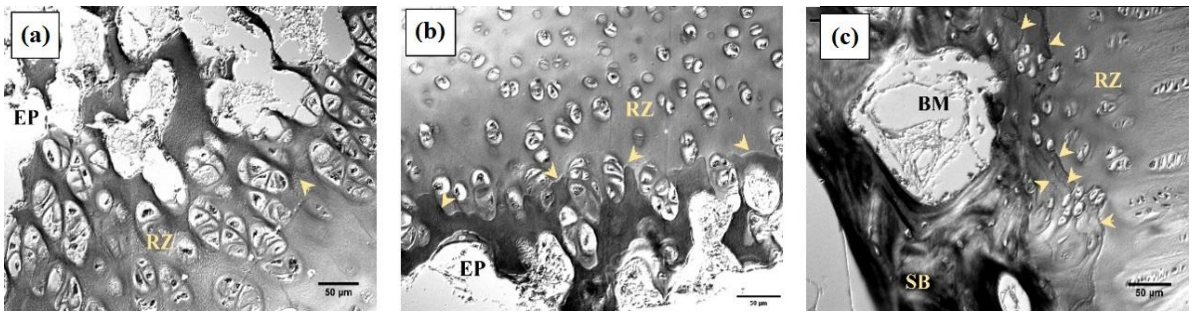

Figure 4: Differential interference contrast images of reserve zone-epiphysis/subchondral bone (RZ-EP/SB) interface by differential interference contrast (DIC) optical microscopy, from the femoral head of (a) 20-, (b) 35-, and (c) 480-day-old pig. Yellow arrowheads point to tidemarks. EP = epiphyseal bone, RZ = reserve zone, SB = subchondral bone, BM = bone marrow.

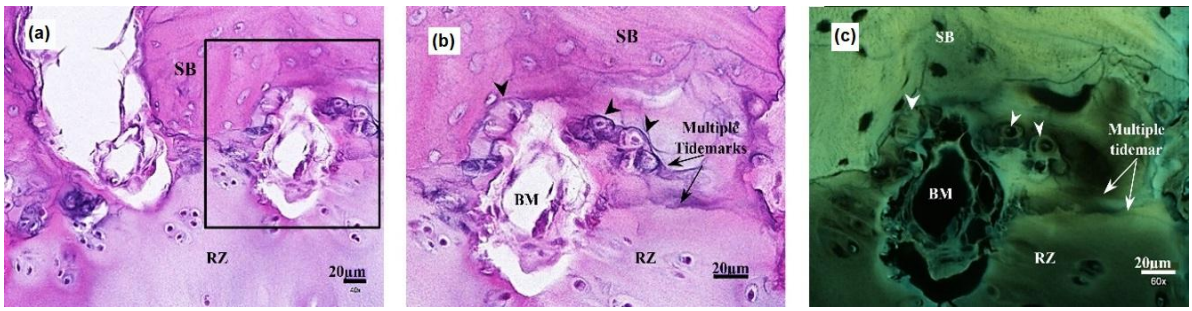

Figure 5: (a) Histology images of the reserve zone-subchondral bone (RZ-SB) interface of the proximal tibial growth plate of yearling bovine calf, stained with H&E, (b) magnified image of black rectangle in (a), (c) fluorescence image of (b) by light microscopy (Keyence, BZ-X710). Arrowheads point to neocartilage cells. RZ = reserve zone, SB = subchondral bone.

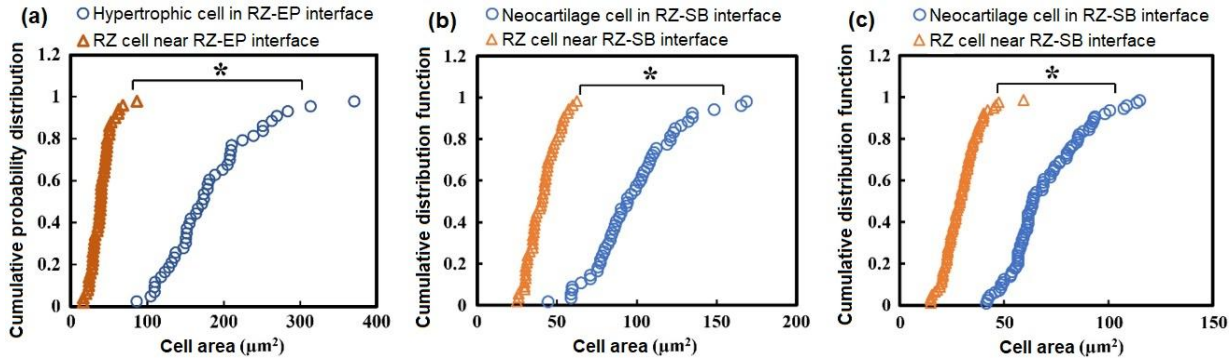

Figure 6: The distribution of cell areas near/within the cartilage-bone interface for (a) 20-, (b) 35-, and (c) 480-day-old pig. *Hypertrophic/neocartilage cells are significantly larger than the reserve zone cell (RzCell) (P-value $< .05$).

regions between bone and the RZ. The results of line scans of the key elements revealed an enhanced intensity of C (Figure 7) and S (not shown) within the RZ. There was also a significant accumulation of Ca and P in the EP/SB region. The line profiles drawn across the cartilage-bone interface presented a chemical gradient of Ca, P, and C across the RZ-EP/SB interface (Figure 7). The average width of the gradient decreased with age so that at 480 days it was on average half the value at 20 days (Table 4 and Figure 8). The gradient transition region between the RZ and EP/SB is demarcated by two red dash-lines in Figure 7. The start and endpoints of the transition zone were delineated based on the backscatter electron (BE) images and the individual smoothed line profiles of the major elements (Ca, P, and C) within the RZ-EP/SB interface, across which Ca/P gradually increased toward the bone side as C decreased (Figures 7(d),

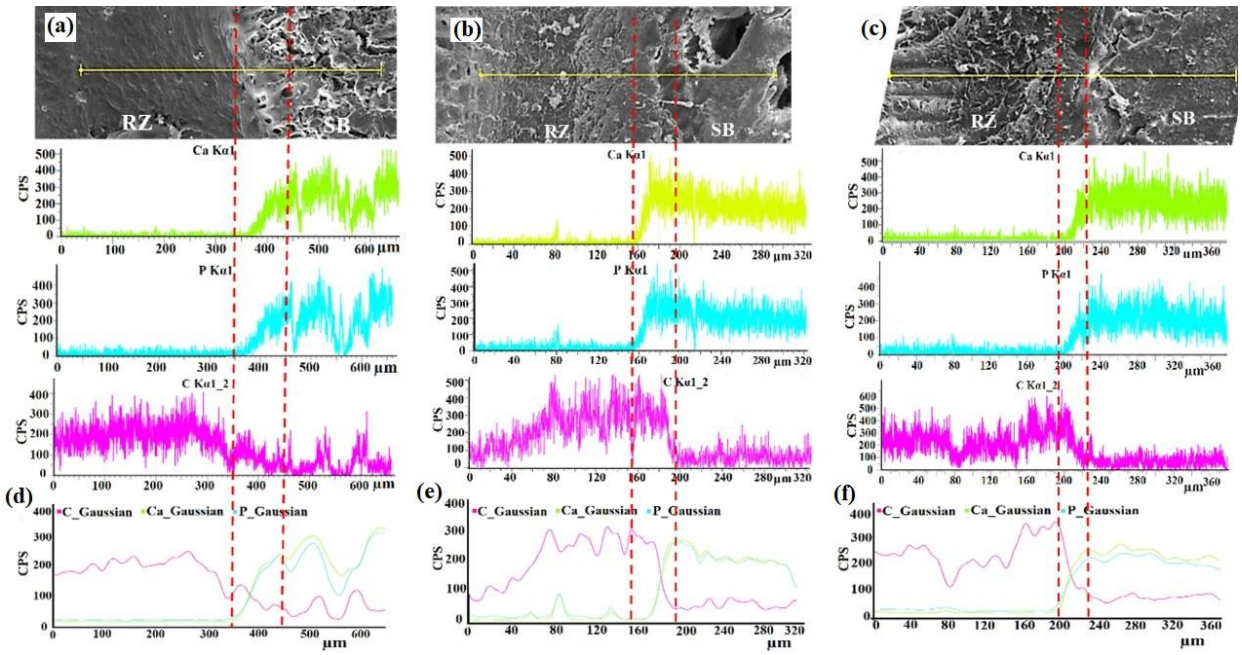

Figure 7: Line profiles taken by EDX across the reserve zone-epiphysis/subchondral bone (RZ-EP/SB) interface for (a) 20-, (b) 35-, and (c) 480-day-old pigs. Vertical red dash lines denote the transition zone between cartilage and bone. The transition zone is determined based on the backscatter image and the EDX line profiles of maximum and minimum values of major elements (Ca, P, and C). (d), (e), and (f) are the smoothed data of (a), (b), and (c), respectively, using a Gaussian filter. CPS = count per second.

Table 4: The results of several line-scans across the RZ-EP/SB interface detected by EDX.

Age group	Parameter		
	The measured chemical transition zone, μm	The mean value of transition zone width, μm	Number of pixels per scanned line
20 days old	38.7	39.6 ± 19.0	317
	35.5		291
	25.8		204
	72.2		99
	26.0		68
35 days old	24.0	29.0 ± 14.3	43
	26.0		213
	17.0		212
	54.0		55
	24.0		100
480 days old	22.0	18.4 ± 4.3	184
	16.0		183
	18.4		151
	16.5		135
	12.9		106
	25.0		86

7(e), and 7(f)). The BE microscopy signals are proportional to the atomic numbers of the scan area; bright gray levels in the BE images indicate mineralized regions with a high concentration of Ca, whereas dark grey levels reflect areas with lower mineral density (Figures 7(a), 7(b), and 7(c)) [44].

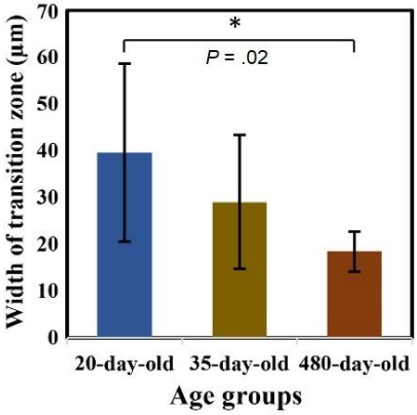

Figure 8: The mean value ($\pm$ Std) of the width of the transition zone between the reserve zone and epiphysis/subchondral bone plate for each age group. *The width of the transition zone at 20 days is significantly larger than that at 480 days (P-value $= .02$).

3.3. Finite element model results

The histology results revealed fundamental changes in the piglet growth plates between 20 and 35 days of age in terms of subchondral bone development and cell morphology at the RZ border. When corresponding finite element models of 20- to 35-day-old growth plates were subjected to compression of 15% of the original growth plate thickness,

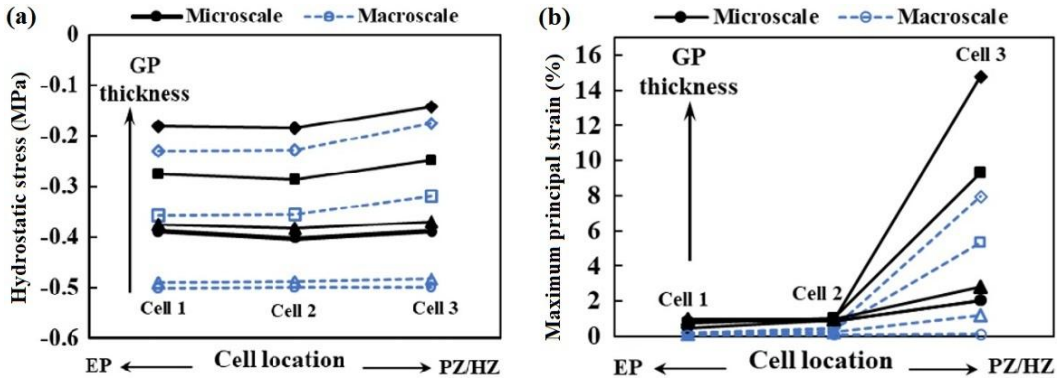

Figure 9: The distribution of (a) depth-dependent cell-averaged hydrostatic stress and (b) maximum principal strain within each cell location for the microscale model in which there are cells and the macroscale model in which there are no cells.

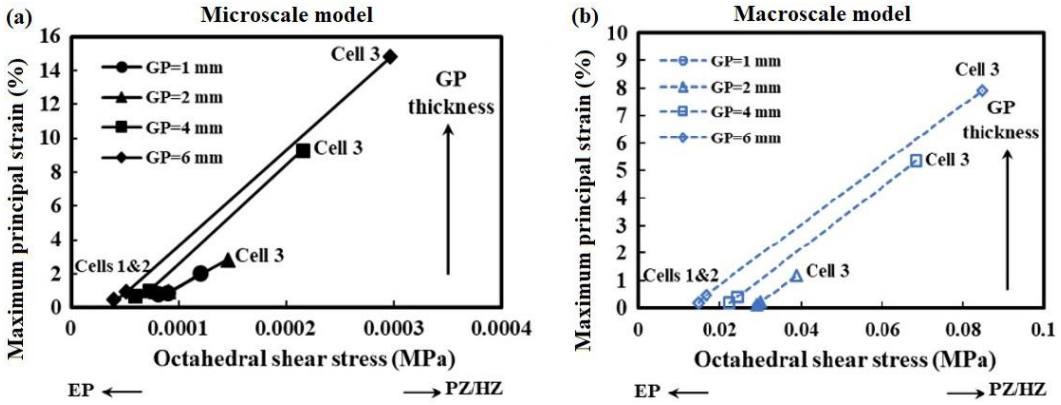

Figure 10: Cell-averaged octahedral shear stress vs maximum principal tensile strain for cells in different locations within the reserve zone moving from epiphysis (EP) to proliferative zone (PZ) subjected to 15% compression of the growth plate cartilage for (a) microscale model and (b) macroscale model in which the material property of ECM was defined for cell geometry.

the results showed a depth-dependent distribution of cell-averaged hydrostatic stresses and maximum principal strains for growth plate (GP) thickness (or widths) values ranging from 1 to 6 mm (Figure 9). The cell-averaged hydrostatic stress at all locations in the RZ increased threefold as the GP thickness decreased from 6 to 1 mm but changed little with cell location within the RZ (Figure 9(a)). As the GP thickness decreased, the cell-averaged maximum tensile strain decreased seven-fold or more at the cell location near the border of the proliferative zone (cell 3) but changed only slightly at the other cell locations within the RZ (Figure 9(b)).

For growth plate thicknesses of 4- and 6-mm the cell-averaged maximum tensile strain for cell 3 increased by about 9 and 15 times, respectively, compared with cells 2 and 1 (Figure 9(b)). Comparing results at different GP thicknesses, cells in a thicker GP experienced lower magnitude of hydrostatic stress and higher maximum principal strain at every location compared with thinner growth plates (Figure 9(a)). Cells near the PZ border in the thickest cartilage had about 63% lower hydrostatic stress than those in the thinnest cartilage. Similar trends were observed for the macroscale model where the cell volumes were assigned to have the same Young's modulus and Poisson's ratio as the surrounding RZ matrix.

Pauwels [20] hypothesized that deviatoric stresses provide a stimulus for differentiation into bone or fibrous connective tissue, and that hydrostatic stresses provide mechanical signals to stimulate the formation of cartilage tissue. In previous modeling studies, which with one exception [23] were all conducted at the tissue level, the proposed stimulus for bone or fibrous connective tissue has sometimes been examined using deviatoric stress [21] and at other times using maximum principal strain [22]. To examine which of these two parameters at the cell level should be evaluated as possible stimuli for bone formation we plotted the relationship between cell volume-averaged maximum principal strains and deviatoric (octahedral shear) stresses for both the micro- and macro-scale models in Figure 10. It can be seen in the both the macro- and micro-scale models that

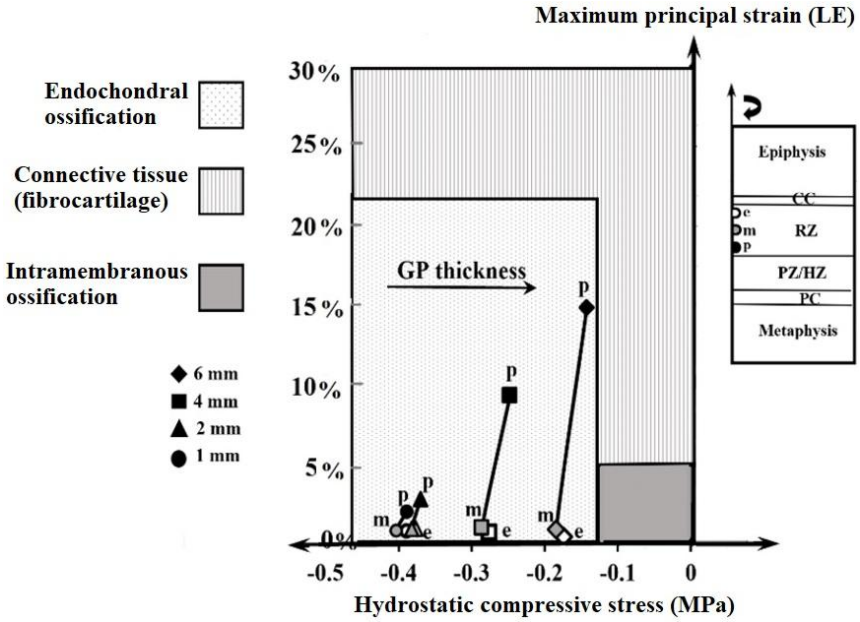

Figure 11: Cell-averaged hydrostatic stress and maximum principal (tensile) strain in reserve zone chondrocytes when the model is subjected to 15% nominal compression. The tissue differentiation phase diagram is similar to one proposed for fracture healing at the tissue macroscale level [22] and for the proliferative and hypertrophic chondrocytes of the growth plate at the cell level [23].

deviatoric (or octahedral) shear stress is accompanied by maximum tensile strain, which demonstrates that even at the cell level Pauwels' hypothesis can be explored using either deviatoric stress or maximum tensile strain.

We plotted the combination of the cell-level mechano-regulatory factors on a tissue differentiation phase diagram to determine if the results are consistent, in qualitative and quantitative terms, with the observed and presumed role of the chondrocytes within the RZ (Figure 11). The combinations of cell volume-averaged mechano-regulatory signals for four different growth plate thicknesses representing thinning of the cartilage with aging, all fell within the region of the diagram that is consistent with endochondral bone formation as shown previously for chondrocytes in the proliferative and hypertrophic zones [23].

4. Discussion

In this study we investigated the hypothesis of a secondary bone growth front at the epiphyseal border of the growth plate that begins after the secondary center of ossification nears completion and that continues into adolescence to form bone in the development of the subchondral bone plate and the mammillary processes. We found a well-developed calcified cartilage layer at the SB/RZ interface with multiple tidemarks and groups of cells at the edge of the calcified border associated with neocartilage and that appeared to become encased in calcified cartilage and occasionally could be seen in proximity to epiphyseal marrow at perforations in the SB plate. These cells bear a resemblance to the chondroprogenitor stem cells that have recently been identified in this location in the reserve zone (Figures 6(b) and 8(g) in [45]) and that can transdifferentiate into multiple cell types including osteoblasts. We showed the existence of a chemical transition zone across the subchondral bone layer between uncalcified cartilage and bone with a gradient in Ca and P indicating the preparation of a calcified cartilage scaffold for subsequent replacement by bone. The width of this transition zone decreased with age as the subchondral bone plate developed ever more undulating patterns to form secondary mammillary processes. Taken together these histological and elemental studies suggest that bone continues to be actively formed at this interface to provide interlocking mammillary processes by a process of endochondral bone formation wherein cartilage is calcified in thin layers that serve as templates for replacement by bone. It also provides evidence that RZ cells calcify the matrix adjacent to the SB and that RZ stem cells may participate in converting this layer into bone. We developed finite element models to show that the mechanical milieu in the RZ is consistent with prevailing quantitative mechanobiological concepts in providing a combination of stress and strain stimuli relevant to endochondral bone formation at both the tissue and cell levels.

4.1. Histology of the RZ/EP interface

At 20 days after birth, hypertrophic cells could be seen at the interface between the RZ cartilage and the chondroepiphysis. At this stage these large cells are

part of the mini growth plate belonging to the secondary ossification center [46,47]. In our results, such hypertrophic cells were found only in the earliest age group, before the completion of growth from the secondary center of ossification and before the formation of the subchondral bone plate. These cells perform a similar function as the cells in the hypertrophic zone near the metaphyseal interface. They disappeared after the SB plate was in the early stages of forming, when a different type of cell was observed, arranged in clusters near nodules of newly formed cartilage (neocartilage). We believe these cells may be stem cells. Between 20 and 35 days the thickness (width) of the RZ decreased dramatically indicating depletion of non-regenerating reserve zone chondrocytes as they are recruited into the proliferative zone. By 35 and 480 days, after the subchondral bone plate began to develop, clusters of cells could be observed, which were closely packed in a basophilic matrix within the RZ-SB interface. These clusters of cells [48] were mostly localized between the tidemarks and bone marrow, which suggests the formation of new cartilage from cells derived either from epiphyseal bone marrow or more likely from stem cells in the RZ that participate in subsequent epiphyseal subchondral bone formation and further development of mamillary processes. The basophilic network of matrix suggests that these cells are differentiating. It has been proposed that such cells could be osteoblast progenitor cells derived from bone marrow [49]. Based on recent studies we might presume that these could also be RZ stem cells, changing their phenotype into osteoblasts to participate in forming an ossification front [24,45,49,50,51,52,53, 54,55]. Mizuhashi et al. (2018) identified some of the reserve zone cells as stem cells by showing that they expressed a panel of markers for skeletal stem/progenitor cells and uniquely possessed the properties as skeletal stem cells in cultured conditions. Cell-lineage analysis also showed that PTHrP-positive chondrocytes in the reserve zone continued to form proliferative chondrocytes, which underwent hypertrophy and became osteoblasts and marrow stromal cells beneath the growth plate [55]. Quantification of the cell areas within the RZ-EP/SB interface for all age groups in our study, also indicated the hypertrophic cells and the cells associated with neocartilage nodules found close to the interface are significantly larger than the areas of RZ chondrocytes more distant from the interface. Our 2D cell area values for cells in locations 2 and 3 are consistent with a previous study [56]. The measured cell radius values, based on the 2D cell area and assuming cells to be circular in shape, are also compatible with a previous study [56].

The appearance of a tidemark by 35 and 480 days indicates that cartilage calcification occurs along the reserve zone border. At 480 days there was evidence of advancing tidemarks which is a sign of a slow ossification front at the RZ/SB interface. Tidemarks along the border of the reserve zone have been noted in a few studies [48,49,57]. Alkaline phosphate (ALP) localization studies have shown the highest values of the ALP secretion to occur at both ends of growth plate cartilage [58]. During active bone growth, the higher value of ALP found at the hypertrophic end of the growth plate is expected. However, localization of ALP at the border of the RZ could be also a further sign of an ossification front. This suggests that the RZ plays a role in the formation of the mammillary processes. Clusters of cells, either arising from the marrow or from the reserve zone are associated with calcified cartilage that appears over time to entrap these cells. The appearance of multiple tidemarks indicates that this is an ongoing process and suggests that it enables the continued evolution of secondary mammillary processes after the initial creation of a subchondral bone plate.

4.2. Elemental gradient at the RZ/EP interface

The SEM/EDX results for the main elemental distribution through the RZ-EP/SB interface were similar in all age groups. In all cases, the concentration of P and Ca, required for hydroxyapatite crystal formation, gradually increased across the cartilage-bone interface, reaching maximum values within the bone region. Conversely, C and S decreased, as expected, from their peak values in cartilage, where C is an essential element for proteoglycan synthesis and C and S are required for collagen/protein production. These results are consistent with previous studies on articular [59,60,61, 62] and growth plate cartilages [27,29,30,63,64]. The gradient of chemical elements associated with mineralization suggests that there is a graded transition in tissue modulus between the stiffer bone tissue and softer cartilage tissue, providing a stress reduction mechanism to the attachment between two structurally and mechanically different tissues. This chemical gradient may also facilitate the transport of small solutes by diffusion thereby enabling crosstalk between calcified cartilage and subchondral bone [65,66]. Such a mechanical transition zone has been reported for the interface between the articular cartilage (AC) and subchondral bone (SB) which has a similar chemical element gradient ranging from 10 to 30 μm in width [67,68] as reviewed elsewhere [42,43]. Our results indicate that the width of the chemical transition zone decreases with age. This age-dependent decrease in the width of the transition zone in the growth plate SB coincides with thinning of the growth cartilage as longitudinal growth slows; and it is accompanied by the formation of secondary mammillary processes that interdigitate across the interface and help reduce the stress concentration. These developments may indicate the beginning stages of eventual epiphyseal fusion when chondrocyte proliferation ceases and another bone plate is formed at the metaphyseal border eventually leading to the replacement of

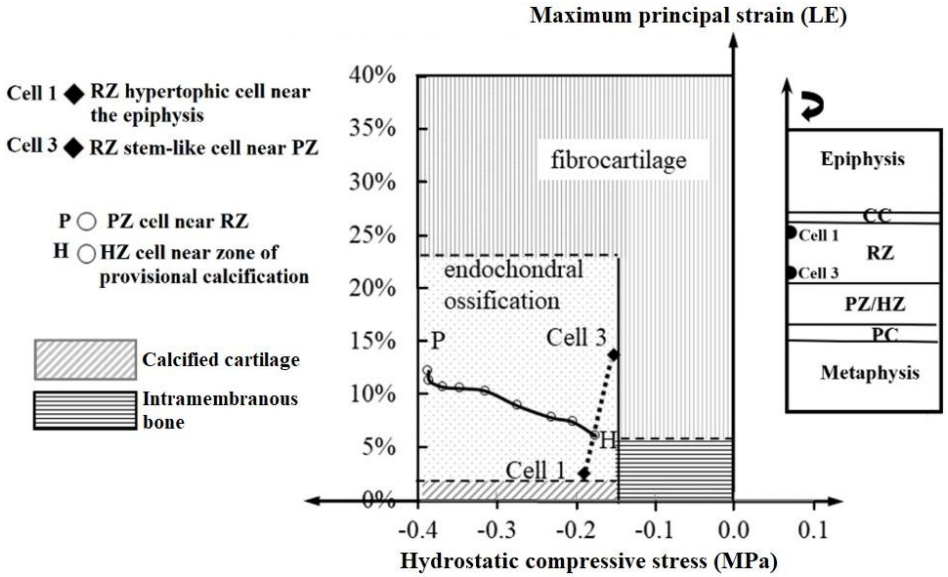

Figure 12: Tissue differentiation diagram showing data from the current study for cells in the RZ under 15% compression of the original growth plate thickness for a 6-mm thick growth plate, along with data from a previous study on cells in the proliferative (P) and hypertrophic (H) zones in a 0.67-mm thick growth plate model subjected to 20% compression. Cell 1 represents a cell at the SB/RZ interface and Cell 3 is a RZ chondrocyte at the border of the PZ. P is a cell at the top of the proliferative zone and H is a cell at the bottom of the hypertrophic zone.

the growth cartilage by well-calcified bone [49]. Similarities in the EDX results and histology patterns between bovine and porcine samples suggests that a dual ossification front exists in many vertebrates including humans.

4.3. Finite element models

We related the mechano-regulatory parameters to the emerging evidence that chondrocytes in the resting zone have two distinct functions: stem cell-like properties as well as the ability to coordinate the orderly differentiation into proliferative and hypertrophic chondrocytes [24,45,50, 51,53,55]. Recent studies [51] provide evidence of a stem cell niche of cells in the reserve zone near the proliferative zone giving rise to chondrocytes that line up and enter the proliferative zone; In addition to biological factors [51] the mechanical environment in and around these stem cells may influence the propensity for recruitment of cells from this stem cell niche. The thickness of the reserve zone decreases with age and this in turn alters the mechanical environment of the RZ cells, including those near the chondroepiphysis border and those adjacent to the proliferative zone. Cell 3 (at the PZ border) experienced higher magnitudes of maximum principal strain and lower magnitudes of hydrostatic stress (Figures 9 and 10) in thicker cartilage, conditions more favorable for proliferation, compared with thinner cartilage. This is consistent with the observation that the rate of bone growth slows with aging (programmed senescence) as the growth plate thickness decreases until growth ceases and cartilage fusion occurs [48,49].

When viewed on a tissue differentiation phase diagram (Figure 11) for each of the four growth plate thickness values the results indicate that the cell-level hydrostatic stress and maximum tensile strain values for all RZ cells fall within the region associated with endochondral ossification (greater than 0.15 MPa of compressive hydrostatic pressure and principal tensile strain values less than 15% strain), as was shown previously at the cell level for cells in the PZ and HZ [23]. Higher maximum principal strain (occurring primarily in the direction perpendicular to column formation) and lower hydrostatic stress, provide a favorable environment for chondrocyte division and this occurs for the cells located closest to the PZ (Cell 3). RZ chondrocytes near the PZ border provide new cells that enter the proliferative zone and this mechanical environment may be favorable for stimulating either non-self-renewing or self-renewing RZ cells into becoming part of or dividing and contributing cells to the proliferative zone in early stages of growth when the growth plate is relatively thick. When the results for Cell 3 in the 6-mm thick growth plate are plotted on a tissue differentiation phase diagram along with the results for cells in the PZ and HZ from a previous study [23] on a 0.67-mm thick growth plate it can be seen that the maximum principal strain for RZ Cell 3 is similar to that for the first chondrocyte in the PZ (P in Figure 12), while the hydrostatic pressure is less than that in proliferative cells. With aging the growth plate gets thinner and the maximum principal strains decrease while hydrostatic stresses increase (Figure 10) creating conditions to keep the

cells in a quiescent state unless they are in the proximity of a blood supply. It can also be observed that Cell 1, located at the RZ/SB interface, has a low maximum principal strain and low hydrostatic pressure in the 6-mm thick growth plate. This is similar to conditions for cells at the end of the HZ (H in Figure 12). This suggests that these mechanical conditions may be favorable not only for calcifying cartilage but for stimulating skeletal stem cells to transdifferentiate into osteoblasts at either the HZ/metaphysis or RZ/SB interfaces in the presence of an adequate source of blood.

We chose a value of 15% compression for this study, which we believe is physiologically relevant. Our elastic model applies to loading at high strain rates for which the mechanical response of the cartilage can be assumed to be time-independent. It has been shown that peak joint loads at the knee during walking are $3 \times$ BW and during jogging $5 \times$ BW [69]. We estimate the average peak nominal stress across a 450-N adolescent proximal tibial growth plate with an area of 2,800 mm^2 to be 0.16 MPa while standing on one leg, 0.48 MPa while walking, and 0.8 MPa during jogging. During heel strike in walking and jogging, strain rates can be estimated to reach 200%/s. We estimate the compressive modulus at 200%/s from the predicted strain-rate dependent behavior of growth plate at 200%/s (Figure 7(a) in [70]) to be around 6 MPa. Using this estimate we can predict peak stresses during heel strike in jogging correspond to peak nominal strain values of about 13%.

The elastic model employed in this study is limited to impact loading for which ignoring the fluid-flow dependent behavior is reasonable when short time durations are compared with stress relaxation times of 1,000 s in compression. Using a biphasic model of the growth plate it has been shown [70] that under impact loading such as heel strike during gait the depth-dependent cell-level strain profile resembles that for a purely elastic solution [42,43].

One of the limitations of this study is our sample size per age group. A larger population would enhance the results. The second limitation concerns the gap in continuity between the 35- and 480-days old samples, which does not provide us with data on how mammillary processes develop within this age gap. Third, the 35-day-old pigs received MTX, a drug used in chemotherapy. This was administered at 14 days and at 4 days before sacrifice. Only the middle age group, the 35-day-old group, was given MTX injections, which could affect bone formation and growth plate thickness depending on the treatment dosage and duration [31,32]. Changes in GP thickness, cell apoptosis and length of tibia have been shown to return to normal at 14 days after injection [34]. In this study the effect of MTX on the bone and cartilage is not clear as we did not have a similar age control group for comparison. However, the histology results showed normal appearing growth plate zones. We believe that although the growth rate may possible have been temporarily interrupted, the data for this group still provide data relevant to an animal with an age between 20- and 480-days old, which is consistent with the aim of this study. Finally, the tissues were stored at $-20\,^{\circ}C$ until use and therefore not suitable for histochemistry studies on the cells at the RZ-SB interface.

5. Conclusions

Our cell-level results indicate that the combination of maximum principal strains and hydrostatic stresses in RZ chondrocytes could predict depth-dependent cell responses. Our results are consistent with tissue level theories in which the combination of mechano-regulatory factors predict tissue differentiation in a tissue differentiation phase diagram of the kind proposed at the tissue level for fracture healing [22] and for the proliferative and hypertrophic zones at the cell level [23]. All the aforementioned evidence suggests that growth plate cartilage has two ossification fronts and two chondro-osseous junctions, one at the HZ border and the other at RZ border with bone. The growth front at the RZ border is responsible for forming the SB plate and either directly or indirectly shaping the mammillary processes. Thus, there may be a third role for the RZ. In addition to providing a niche of stem cells and coordinating the formation of the PZ and HZ, the RZ also appears to actively form the SB plate and may be responsible for forming a robust interdigitating interface with a uniform thickness of growth cartilage.

Funding This research did not receive any specific grant from funding agencies in the public, commercial, or not-for-profit sectors.

Acknowledgments The authors thank Dr. Omar Skalli, Dr. Felio Perez and Lauren Thompson at the University of Memphis Integrated Microscopy Center for their help with histology and SEM/EDX studies and their technical assistance. We gratefully thank Dr. Robert Read for his advice on histology and sample preparation. We thank Dr. Aaryani Sajja for advice on signal analysis. We thank Dr. Randal Buddington for providing us with piglet bones at the University of Memphis.

Conflict of interest The authors declare that they have no conflict of interest.

References

[1] B. Cohen, G. S. Chorney, D. P. Phillips, H. M. Dick, J. A. Buckwalter, A. Ratcliffe, et al., *The microstructural tensile properties and biochemical composition of the bovine distal femoral growth plate*, J Orthop Res, 10 (1992), 263–275.

[2] J. L. Williams, J. N. Vani, J. D. Eick, E. C. Petersen, and T. L. Schmidt, *Shear strength of the physis varies with anatomic location and is a function of modulus, inclination, and thickness*, J Orthop Res, 17 (1999), 214–222.

[3] J. Gao, J. L. Williams, and E. Roan, *On the state of stress in the growth plate under physiologic compressive loading*, Open J Biophys, 4 (2014), 13–21.

[4] J. W. Smith, *The relationship of epiphysial plates to stress in some bones of the lower limb*, J Anat, 96 (1962), 58–78.

[5] C. Barrios, M. A. Blasco, M. C. Blasco, and J. Gascó, *Posterior sloping angle of the capital femoral physis: a predictor of bilaterality in slipped capital femoral epiphysis*, J Pediatr Orthop, 25 (2005), 445–449.

[6] S. Hosseinzadeh, A. M. Kiapour, D. A. Maranho, S. A. Emami, G. Portilla, Y. J. Kim, et al., *The metaphyseal fossa surrounding the epiphyseal tubercle is larger in hips with moderate and severe slipped capital femoral epiphysis than normal hips*, J Child Orthop, 14 (2020), 184–189.

[7] R. Liu, D. Armstrong, A. Levine, A. Gilmore, G. Thompson, and D. Cooperman, *An anatomic study of the epiphyseal tubercle and its importance in the pathogenesis of slipped capital femoral epiphysis*, J Bone Joint Surg Am, 95 (2013), e34.

[8] R. T. Loder, *Slipped capital femoral epiphysis*, Am Fam Physician, 57 (1998), 2135–2142.

[9] E. M. Manoff, M. B. Banffy, and J. J. Winell, *Relationship between Body Mass Index and slipped capital femoral epiphysis*, J Pediatr Orthop, 25 (2005), 744–746.

[10] A. L. Lerner and J. L. Kuhn, *Characterization of regional and age-related variations in the growth of the rabbit distal femur*, J Orthop Res, 15 (1997), 353–361.

[11] A. L. Lerner, J. L. Kuhn, and S. J. Hollister, *Are regional variations in bone growth related to mechanical stress and strain parameters?*, J Biomech, 31 (1998), 327–335.

[12] M. Kazemi and J. L. Williams, *Elemental and histological study of the growth plate reserve zone-subchondral bone interface*, Paper presented at the Orthopaedic Research Society Annual Meeting, New Orleans, LA, 2018.

[13] D. P. Speer and L. Dahners, *The collagenous architecture of articular cartilage: Correlation of scanning electron microscopy and polarized light microscopy observations*, Clin Orthop Relat Res, 1979 (1979), 267–275.

[14] N. D. Broom and C. A. Poole, *A functional-morphological study of the tidemark region of articular cartilage maintained in a non-viable physiological condition*, J Anat, 135 (1982), 65–82.

[15] D. P. Speer, *Collagenous architecture of the growth plate and perichondrial ossification groove*, J Bone Joint Surg Am, 64 (1982), 399–407.

[16] C. Hueter, *Anatomische Studien an den Extremitätengelenken Neugeborener und Erwachsener*, Arch Pathol Anat Physiol Klin Med, 25 (1862), 572–599.

[17] R. V. Volkmann, *Verletzungen und Krankheiten der Bewegungsorgane*, in Handbuch der allgemeinen und speziellen Chirurgie, Enke, Stuttgart, 1882, 412.

[18] D. R. Carter and M. Wong, *Mechanical stresses and endochondral ossification in the chondroepiphysis*, J Orthop Res, 6 (1988), 148–154.

[19] H. M. Frost, *Skeletal structural adaptations to mechanical usage (SATMU): 3. The hyaline cartilage modeling problem*, Anat Rec, 226 (1990), 423–432.

[20] F. Pauwels, *Eine neue theorie über den Einfluß mechanischer Reize auf die Differenzierung der Stützgewebe*, Z Anat Entwicklungsgesch, 121 (1960), 478–515.

[21] D. R. Carter and G. S. Beaupré, *Skeletal Function and Form: Mechanobiology of Skeletal Development, Aging, and Regeneration*, Cambridge University Press, Cambridge, 2000.

[22] L. E. Claes and C. A. Heigele, *Magnitudes of local stress and strain along bony surfaces predict the course and type of fracture healing*, J Biomech, 32 (1999), 255–266.

[23] J. Gao, J. L. Williams, and E. Roan, *Multiscale modeling of growth plate cartilage mechanobiology*, Biomech Model Mechanobiol, 16 (2017), 667–679.

[24] J. C. Lui, *Home for a rest: stem cell niche of the postnatal growth plate*, J Endocrinol, 246 (2020), R1–R11.

[25] A. J. D'Alfonso, B. Freitag, D. Klenov, and L. J. Allen, *Atomic-resolution chemical mapping using energy-dispersive x-ray spectroscopy*, Phys Rev B, 81 (2010), 100101.

[26] D. Wollman, K. Irwin, G. Hilton, L. Dulcie, D. Newbury, and J. Martinis, *High-resolution, energy-dispersive microcalorimeter spectrometer for X-ray microanalysis*, J Microsc, 188 (1997), 196–223.

[27] A. Boyde and I. M. Shapiro, *Energy dispersive X-ray elemental analysis of isolated epiphyseal growth plate chondrocyte fragments*, Histochemistry, 69 (1980), 85–94.

[28] R. Gangadhar, K. A. Jaleeli, and A. Ahmad, *Energy dispersive x-ray analysis of ovine scapular cartilage*, Int J Sci Env Technol, 4 (2015), 1195–1198.

[29] I. M. Shapiro and A. Boyde, *Microdissection—elemental analysis of the mineralizing growth cartilage of the normal and rachitic chick*, Metab Bone Dis Relat Res, 5 (1984), 317–326.

[30] K. Takata, K. Yamamoto, S. Ohmori, and T. Watanabe, *Scanning electron microscopic study and elemental analysis of the epiphyseal growth plate in normal puppies*, Orthop Traumatol, 23 (1974), 44–47.

[31] S. C. Cavalcanti, L. Corrêa, S. B. Mello, and J. G. Luz, *The effect of methotrexate on the bone healing of mandibular condylar process fracture: an experimental study in rats*, J Craniomaxillofac Surg, 42 (2014), 1133–1139.

[32] C. Fan, J. C. Cool, M. A. Scherer, B. K. Foster, T. Shandala, H. Tapp, et al., *Damaging effects of chronic low-dose methotrexate usage on primary bone formation in young rats and potential protective effects of folinic acid supplementary treatment*, Bone, 44 (2009), 61–70.

[33] B. L. Van Leeuwen, G. J. Verkerke, R. M. Hartel, W. J. Sluiter, W. A. Kamps, H. W. Jansen, et al., *Chemotherapy decreases epiphyseal strength and increases bone fracture risk*, Clin Orthop Relat Res, 2003 (2003), 243–254.

[34] C. Xian, J. Cool, M. Scherer, C. Macsai, C. Fan, M. Covino, et al., *Cellular mechanisms for methotrexate chemotherapy-induced bone growth defects*, Bone, 41 (2007), 842–850.

[35] G. Landini, *How to correct background illumination in brightfield microscopy*, available at: https://imagejdocu.list.lu/howto/working/how_to_correct_background_illumination_in_brightfield_microscopy.

[36] C. Schneider, W. Rasband, and K. Eliceiri, *NIH Image to ImageJ: 25 years of image analysis*, Nat Methods, 9 (2012), 671–675.

[37] S. S. Stevens, G. S. Beaupré, and D. R. Carter, *Computer model of endochondral growth and ossification in long bones: biological and mechanobiological influences*, J Orthop Res, 17 (1999), 646–653.

[38] J. Gao, E. Roan, and J. L. Williams, *Regional variations in growth plate chondrocyte deformation as predicted by three-dimensional multi-scale simulations*, PLoS One, 10 (2015), e0124862.

[39] D. M. Allen and J. J. Mao, *Heterogeneous nanostructural and nanoelastic properties of pericellular and interterritorial matrices of chondrocytes by atomic force microscopy*, J Struct Biol, 145 (2004), 196–204.

[40] F. Guilak, A. Ratcliffe, and V. C. Mow, *Chondrocyte deformation and local tissue strain in articular cartilage: a confocal microscopy study*, J Orthop Res, 13 (1995), 410–421.

[41] V. Lešer, M. Milani, F. Tatti, Z. P. Tkalec, J. Strus, and D. Drobne, *Focused ion beam (FIB)/scanning electron microscopy (SEM) in tissue structural research*, Protoplasma, 246 (2010), 41–48.

[42] M. Kazemi and J. L. Williams, *Chondrocyte and pericellular matrix deformation and strain in the growth plate cartilage reserve zone under compressive loading*, in Computer Methods, Imaging and Visualization in Biomechanics and Biomedical Engineering. CMBBE 2019, G. Ateshian, K. Myers, and J. Tavares, eds., vol. 36 of Lecture Notes in Computational Vision and Biomechanics, Springer-Verlag, Cham, 2020.

[43] M. Kazemi and J. L. Williams, *Properties of cartilage-subchondral bone junctions: A narrative review with specific focus on the growth plate*, Cartilage (to appear).

[44] D. A. Bradley, M. J. Farquharson, O. Gundogdu, A. Al-Ebraheem, E. C. Ismail, W. Kaabar, et al., *Applications of condensed matter understanding to medical tissues and disease progression: Elemental analysis and structural integrity of tissue scaffolds*, Radiat Phys Chem, 79 (2010), 162–175.

[45] P. T. Newton, L. Li, B. Zhou, C. Schweingruber, M. Hovorakova, M. Xie, et al., *A radical switch in clonality reveals a stem cell niche in the epiphyseal growth plate*, Nature, 567 (2019), 234–238.

[46] C. E. Farnum and N. J. Wilsman, *Morphologic stages of the terminal hypertrophic chondrocyte of growth plate cartilage*, Anat Rec, 219 (1987), 221–232.

[47] L. I. Hansson, K. Menander-Sellman, A. Stenström, and K.-G. Thorngren, *Rate of normal longitudinal bone growth in the rat*, Calcif Tissue Res, 10 (1972), 238–251.

[48] R. W. Haines, *The histology of epiphyseal union in mammals*, J Anat, 120 (1975), 1–25.

[49] A. M. Parfitt, *Misconceptions (1): epiphyseal fusion causes cessation of growth*, Bone, 30 (2002), 337–339.

[50] V. Abad, J. L. Meyers, M. Weise, R. I. Gafni, K. M. Barnes, O. Nilsson, et al., *The role of the resting zone in growth plate chondrogenesis*, Endocrinology, 143 (2002), 1851–1857.

[51] S. A. Hallett, W. Ono, and N. Ono, *Growth plate chondrocytes: Skeletal development, growth and beyond*, Int J Mol Sci, 20 (2019), 6009.

[52] A. S. Hammond, J. Ning, C. V. Ward, and M. J. Ravosa, *Mammalian limb loading and chondral modeling during ontogeny*, Anat Rec (Hoboken), 293 (2010), 658–670.

[53] C. H. Killion, E. H. Mitchell, C. G. Duke, and R. Serra, *Mechanical loading regulates organization of the actin cytoskeleton and column formation in postnatal growth plate*, Mol Biol Cell, 28 (2017), 1862–1870.

[54] Y. Matsushita, W. Ono, and N. Ono, *Growth plate skeletal stem cells and their transition from cartilage to bone*, Bone, 136 (2020), 115359.

[55] K. Mizuhashi, W. Ono, Y. Matsushita, N. Sakagami, A. Takahashi, T. L. Saunders, et al., *Resting zone of the growth plate houses a unique class of skeletal stem cells*, Nature, 563 (2018), 254–258.

[56] S. Amini, D. Veilleux, and I. Villemure, *Three-dimensional in situ zonal morphology of viable growth plate chondrocytes: a confocal microscopy study*, J Orthop Res, 29 (2011), 710–717.

[57] C. D. Hoemann, C. H. Lafantaisie-Favreau, V. Lascau-Coman, G. Chen, and J. Guzmán-Morales, *The cartilage-bone interface*, J Knee Surg, 25 (2012), 85–97.

[58] D. Miao and A. Scutt, *Histochemical localization of alkaline phosphatase activity in decalcified bone and cartilage*, J Histochem Cytochem, 50 (2002), 333–340.

[59] W. Kaabar, O. Gundogdu, D. A. Bradley, O. Bunk, F. Pfeiffer, F. Pfeiffer, et al., *Compositional studies at the Bone-Cartilage interface using PIXE, RBS and cSAXS techniques*, in Proceedings of the Ninth Radiation Physics and Protection Conference, Cairo, Egypt, 2009, 359–369.

[60] W. Kaabar, E. Daar, O. Gundogdu, P. M. Jenneson, M. J. Farquharson, M. Webb, et al., *Metal deposition at the bone-cartilage interface in articular cartilage*, Appl Radiat Isot, 67 (2009), 475–479.

[61] W. Kaabar, E. Daar, O. Bunk, M. J. Farquharson, A. Laklouk, M. Bailey, et al., *Elemental and structural studies at the bone-cartilage interface*, Nucl Instrum Methods Phys Res A, 652 (2011), 786–790.

[62] W. Kaabar, O. Gundogdu, A. Laklouk, O. Bunk, F. Pfeiffer, M. J. Farquharson, et al., *μ-PIXE and SAXS studies at the bone-cartilage interface*, Appl Radiat Isot, 68 (2010), 730–734.

[63] J. Althoff, P. Quint, E. R. Krefting, and H. J. Höhling, *Morphological studies on the epiphyseal growth plate combined with biochemical and X-ray microprobe analyses*, Histochemistry, 74 (1982), 541–552.

[64] F. Vittur, C. Tuniz, S. Paoletti, R. Rizzo, and K. W. Jones, *Elemental analysis of growth plate cartilage by synchrotron-radiation-induced X-ray emission (SRIXE)*, Biochem Biophys Res Commun, 188 (1992), 1010–1017.

[65] K. P. Arkill and C. P. Winlove, *Solute transport in the deep and calcified zones of articular cartilage*, Osteoarthritis Cartilage, 16 (2008), 708–714.

[66] P. M. Gribbon, A. Maroudas, K. H. Parker, and C. P. Winlove, *Water and solute transport in the extracellular matrix: physical principles and macromolecular determinants*, in Connective Tissue Biology: Integration and Reductionism, R. K. Reed and K. Rubin, eds., Portland Press, London, 1998, 95–124.

[67] S. E. Campbell, V. L. Ferguson, and D. C. Hurley, *Nanomechanical mapping of the osteochondral interface with contact resonance force microscopy and nanoindentation*, Acta Biomater, 8 (2012), 4389–4396.

[68] H. S. Gupta, S. Schratter, W. Tesch, P. Roschger, A. Berzlanovich, T. Schoeberl, et al., *Two different correlations between nanoindentation modulus and mineral content in the bone-cartilage interface*, J Struct Biol, 149 (2005), 138–148.

[69] G. Bergmann, A. Bender, F. Graichen, J. Dymke, A. Rohlmann, A. Trepczynski, et al., *Standardized loads acting in knee implants*, PLoS One, 9 (2014), e86035.

[70] M. Kazemi and J. L. Williams, *Depth and strain rate-dependent mechanical response of chondrocytes in reserve zone cartilage subjected to compressive loading*, Biomech Model Mechanobiol (2021).